Circular Economy and Sustainability (2026) 6:99
https://doi.org/10.1007/s43615-026-00880-9

ORIGINAL PAPER

Decoating of TiN-Coated Cemented Tungsten Carbide Tools by Laser Ablation for Remanufacturing Purposes

Oliver Maurer[1] · **Roger Escolano Benach**[1] · **Dirk Bähre**[1]

Received: 9 September 2025 / Accepted: 2 March 2026

Abstract
Cutting technologies are in wide industrial use and rely on durable tools to machine as many parts as possible before the tool is worn out. Cemented carbide tools such as indexable inserts provide several cutting edges and are readily replaceable by new ones. They consist of a cemented carbide body with hard coatings of oxide or non-oxide ceramics. The cemented carbide body consumes large amounts of energy in several sintering stages at its begin of life. In order to save energy and resources that would be required to manufacture new inserts, it would promote sustainability to remanufacture and recondition used inserts and, by that, maintain the cemented carbide body. Therefore, this study aims to remove hard non-oxide ceramic coatings from the cemented carbide with a commercially available laser engraving system. Laser ablation offers less geometrical constraints than machining approaches and does not depend on the hardness of the coating. As a result, this study offers suitable laser ablation parameters to remove TiN coatings from commercially available inserts and proves that this process consumes less energy than producing new inserts. This gives the opportunity to selectively decoat and recondition indexable inserts in the future. Thereby, the energy-intensive production of new cemented carbide bodies is avoided allowing the cutting technology to reach higher sustainability goals.

Keywords Cemented carbide tools · Laser ablation · Remanufacturing · Decoating

Roger Escolano Benach and Dirk Bähre contributed equally to this work.

✉ Oliver Maurer
oliver.maurer@uni-saarland.de

Dirk Bähre
lft@mx.uni-saarland.de

[1] Institute of Production Engineering, Saarland University, Campus A5.1, Saarbrücken 66123, Saarland, Germany

Published online: 11 March 2026

Introduction

Wear resistant tools drive numerous machining operations such as milling, turning and drilling of metals [29]. Their hardness increases the machining efficiency due to a long tool service life [10]. Hard and wear resistant tools to machine metals are often fabricated from cemented carbides, a composite material of tungsten carbide (WC) particles embedded in a metallic matrix, usually cobalt (Co) [32]. The metallic matrix increases a cemented carbide tool's toughness if compared to very hard but rather brittle ceramic tools [10, 18]. However, the compromise between hardness and toughness of cemented carbide tools does not prevent regular replacements after a designated time of operation or predefined occurrence of wear. Different types of wear can serve as criteria to terminate a tool's use phase. Common types of wear are for instance flank wear on cutting edges [44] or crater wear on rake faces [45]. These phenomena correspond to abrasive wear mechanisms [29]. Furthermore, there are mechanisms of adhesion, diffusion, tribochemical reactions and contact fatigue [43]. Chosen parameters of the machining process, its kinematics and the chosen tool geometry influence the specific wear behavior [1, 26, 31].

Thin coatings of oxide or non-oxide ceramics can extend the service life of cemented carbide tools [10, 29]. Physical or chemical vapor deposition (PVD and CVD) are well established methods to coat tools [27]. Using these techniques, titanium carbide (TiC), titanium nitride (TiN), titanium aluminum nitride ($Ti_xAl_{1-x}N$) and alumina (Al_2O_3) are commonly applied on numerous types of tool geometries [28]. Chemical composition and sequence of coating layers affect the observed wear behavior by adjusting mechanical properties [34]. Nevertheless, the same macroscopic wear phenomena as with uncoated tools are reported in the literature review of [42].

Sustainability and circularity of coated cemented carbide tools was subject to several studies. It is well known in machining that wear-resistance of tools increases their service life, enhances in turn the cost efficiency and reduces labor [29]. [17] conducted a life-cycle assessment of coated and uncoated cemented carbide tools and emphasized the potentials of recycling by means of environmental impacts. With their coating material of interest, polycrystalline diamond, coated tools performed better during the use phase whereas uncoated tools performed better in recycling. Recycling technologies of cemented carbide tools are established to recover the valuable materials used. Usually, worn out tools are crushed, shredded and ground or ball milled to reach a particle size where subsequent processes can separate WC and Co from each other [15, 52]. After separation and cleaning, recycled powders can be produced to fabricate new tools. Shortening the loop can reduce processing costs and environmental impacts at once [2]. So, removing the coating from a worn out cemented carbide tool body becomes a key to achieve shorter remanufacturing loops at the longest use phase. Hardness values in the range of 27 GPa [24] for TiN or several thousands HV [27] for other ceramic coatings make it complex but not impossible to decoat by grinding [33]. Especially tooling costs and the ever existing grinding tool wear mark major drawbacks of decoating by grinding as described in [14, 37]. First, the coating has to be removed. Chemical etching using either hydrogen peroxide (H_2O_2) [5, 49] or reactive ion etching [50] can remove coating sufficiently and precisely. However, etching leads to long decoating processes and decoats every surface which stays in contact with the etching media. Additionally, as indicated by [50], hazardous substances such as sulfur hexafluoride (SF_6) or chlorine based reactants are required to decoat ceramics from cemented carbide. In

order to overcome these drawbacks, laser selective ablation of definable portions of surface areas are investigated. Laser technologies offer to decoat complex tool geometries which are adjusted to specific applications like drill bits properly [7]. Researchers used lasers from the ultraviolet (UV) to the infrared (IR) part of the spectrum. The experiments in literature often focus on samples from laboratory coating processes and no commercially available tools. As Table 1 indicates, various decoating setups were presented in literature. Ultraviolet lasers usually operate in a cold mode of photo-chemical ablation, whereas infrared lasers rely on the photo-thermal ablation including melting and vaporization [22]. Most listed publications ablated coatings from different types of substrates. Only [21] used laser ablation to recondition cutting edges of an uncoated cemented carbide tool which was worn out by crater wear.

Laser ablation is a suitable technology for decoating but must not emit hazardous substances to contribute to sustainable remanufacturing. There are no studies available which investigate the nature of ablation products of relevant tool coatings. However, it is well established that the process of laser ablation of ceramics emits nano particles [16], since laser ablation is used to produce TiN nanoparticles which tend to agglomerate irregularly [38]. TiN may oxidize [19], e.g. during laser ablation in a thermal mode. As reported by [51], laser degradation of TiN includes the formation of gaseous nitrogen and metallic titanium which subsequently oxidizes to TiO_2. Generally, titanium-based non-oxide and oxide ceramics TiN, TiC, TiCN and Ti_xO_y as bulk materials or as powders are not considered toxic or hazardous but persist in aqueous media as industrial material safety data sheets prove [9, 23, 25, 35, 48]. Therefore, operators must be protected from inhalable particles and ablation products must be kept away from ground water or the municipal sewage and fresh water systems. If a laser machine is equipped with a filtered exhaust ventilation, environmental impacts are not to be expected in laser decoating of cemented carbide tools.

This study aims to contribute to shorter remanufacturing cycles of coated cemented carbide tools by decoating unused indexable inserts for milling with laser ablation using a low power laser engraving system operating in the infrared spectrum. The maximum power of this laser engraving system is 30 W with 250 ns pulse duration which equals

Table 1 Experimental specifications presented in literature to remove ceramic coatings by laser ablation

Coating material	Substrate material	Laser type	Laser power or pulse energy	Reference
TiAlN	cemented carbide	UV excimer	N/A	[36]
TiN	WC	UV excimer	560 mJ	[46]
TiN	tool steel	IR fiber	3.4 kW	[11]
TiN	steel	UV, VIS, IR	various	[30]
AlTiN	tool steel	IR solid state	50 W	[39]
AlTiN	cemented carbide	IR femtosecond	40 W	[40]
TiAlN	cemented carbide	VIS picosecond	12 W	[7]
Diamond-like carbon	cemented carbide	UV excimer	560 mJ	[3]
None	cemented carbide	IR fiber	70 W	[20]

a pulse energy of 7.5 μJ. Hence, energy savings during laser decoating are achieved. Indexable inserts as small and low-cost cemented carbide tools with coatings are chosen as representatives. It is assumed that if indexable inserts are suitable for remanufacturing, tools with higher consumption of primary raw materials are also suitable. For the first time, optimized the remanufactured cemented carbide body after laser ablation, which acts as a secondary resource, is compared to the production of an equal cemented carbide body from primary resources by means of energy consumption and thus green house gas emissions. So, this study enters the question whether the laser decoating route to remanufacture tools is valid from an ecological perspective and whether this route can maintain the integrity of cemented carbide bodies.

Materials and Methods

Coated Tools used and their Properties

New TiN-coated milling inserts model Garant HB7525 without circumferential chip breakers (Hoffmann SE, Munich, Germany) were chosen for the experiments. This simple geometry corresponds to the SEKN 1203 AFTN specification. Figure 1 contains digital a microscopy image and a technical drawing of this insert type.

To assess the coating thickness, one insert was cut on a Minitom (Struers, Copenhagen, Denmark) equipped with a diamond-coated blade. Both halves were embedded in resin, polished with successively finer grit sandpaper (600/1200/2000) and with 3 μm diamond suspension followed by 1 μm diamond suspension. After polishing, they were etched using Murakami's reagent for 70 s, after which they were cleaned with water. Then, SEM analysis was carried out with a Sigma VP SEM (Zeiss AG, Oberkochen, Germany) in secondary electron (SE) and backscattered electron (BSE) modes to measure the coating thickness properly. As the electron microscope also incorporated EDX capabilities, a chemical analysis was conducted of the samples in order to verify the composition of substrate and

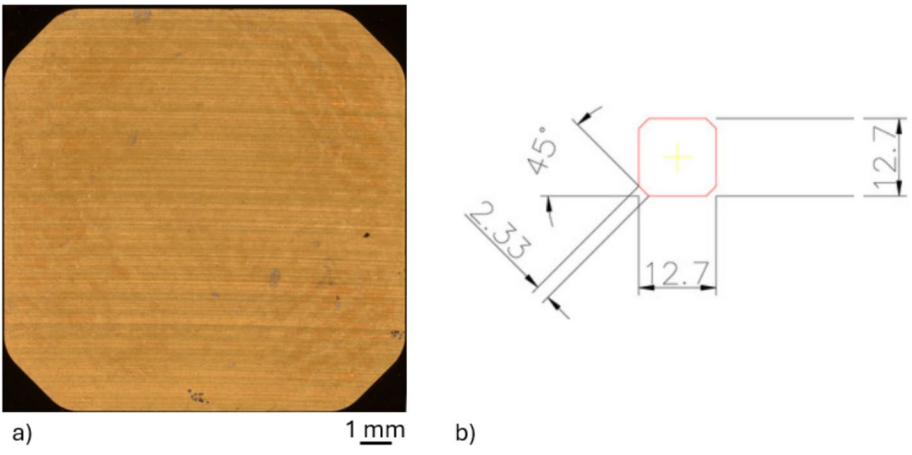

Fig. 1 **a**) TiN-coated milling insert SEKN 1203 AFTN and **b**) technical drawing provided by the manufacturer, edge lengths given in mm

coating. This enables to make diffusion zones visible at the boundary between TiN-coating and WC-body. Therefore, line spectra and point spectra were recorded to distinguish the Co-matrix from WC-particles and the TiN-coating.

Laser Engraving System for Decoating

The laser used in this study is a Strasor Advanced (Mobil-Mark GmbH, St. Ingbert, Germany). Table 2 summarizes its specifications. Along with its control software and presets, custom parameter sets can be adjusted to each specific application. Its maximum scan area without using its 2D stage measures 110 mm by 110 mm. Additionally, this laser offers an automatic focus control, so topographies on tools may be ablated in the same manner as even surfaces. The scan pattern consists of meandering tracks, which have no length limitation.

This laser engraving system reaches a peak fluence per pulse of $F = 0.38\ \frac{\mathrm{J}}{\mathrm{cm}^2}$ exceeding the ablation threshold of TiN $F_{th} = 0.28\ \frac{\mathrm{J}}{\mathrm{cm}^2}$ adapted from [6]. The fluence exceeds the threshold value by a factor of ≈ 1.36.

The specs of Table 2 serve as parameters to adjust to laser decoating and partially contribute to the calculation of the NOP. First tests focused on decoating squares which measure 1.2 mm by 1.2 mm. Additionally, several scans may decoat tools more suitably than only one. This makes the angle increment between scans another factor to affect the ablation quality. An angle increment of $22.5°$ allows to stack 16 scans until the initial scan pattern orientation repeats. If the initial scan orientation at $n = 1$ refers to $0°$, the total rotation angle θ in a subsequent scan $n > 1$ is $\theta = (n-1) * 22.5°$. Additionally, the control software of this engraving laser system records the duration t_{on} an entire scan takes until completion. This allows to calculate the rate of decoating r_{decoat} an area A entirely as per $r_{decoat} = \frac{A}{t_{on}}$. Based on these conditions, the parameter study of Table 3 was designed. Its first two sections show parameter adjustments to vary the NOP omitting and using multiple scans per area. The third section bases on the first one and enters the dependency on the pulse frequency. In this section, the scan speed is adjusted and offsets are kept constant to maintain a NOP of 8 or 16, respectively.

Ablation Characterization Techniques

Several characterization techniques helped to analyze the quality of laser decoating. Ablation depth as well as surface roughness of ablated and unablated areas was measured optically with a digital microscope VHX 7000 (Keyence Corp., Osaka, Japan) at a minimum magnification of 700 to resolve small features properly. Micrographs that provide overviews were recorded with smaller magnifications. Scans of larger areas got stitched together by the VHX 7000 software by its 2D or 3D panorama functions allowing to measure the surface roughness. Again SEM imaging assured that ablation removed the entire thickness of a coating in BSE mode and by using EDX. Therefore, the same SEM setup as described before was used.

Table 2 Specification of the Strasor Advanced laser used to decoat the inserts

Max. power /W	Wave-length /nm	Max. pulse frequency / kHz	Pulse duration /ns	Beam width /μm & Beam profile
30	1098	50	250	50 Gaussian

Table 3 Studied parameter variation at the maximum power of 30 W; f: laser pulse frequency, v: laser scan speed, Δx and Δy: offset to neighboring laser spot along and perpendicular to scan direction, n: number of scans (angle increment = 22.5° if $n > 1$), NOP_{scan}: number of pulses per scan without rotating by 22.5°, NOP_{total}: number of pulses including scan repetitions, r_{decoat}: calculated decoating rate, F_{spot}: fluence exposure per spot according to NOP_{scan}

f/kHz	v/mm/s	Δx/%	Δy/%	n/-	NOP_{scan}/-	NOP_{total}/-	r_{decoat}/cm²/s	F_{spot}/J/cm²
30	1155	70	70	1	2	2	0.43	0.76
30	825	50	50	1	4	4	0.23	1.52
30	674	40.8	40.8	1	6	6	0.15	2.28
30	584	35	35	1	8	8	0.11	3.04
30	522	32	32	1	10	10	0.09	3.80
30	412	25	25	1	16	16	0.06	6.08
30	292	18	18	1	32	32	0.03	12.16
30	1155	70	70.7	2	2	4	0.22	0.76
30	825	50	50	2	4	8	0.11	1.52
30	1155	70	70.9	4	2	8	0.11	0.76
30	674	40.8	35.3	2	7	14	0.07	2.66
30	825	50	50	4	4	16	0.06	1.52
30	1155	70	70.9	8	2	16	0.06	0.76
30	412	25	25	2	16	32	0.03	6.08
30	825	50	50	8	4	32	0.03	1.52
30	583	35.4	35.4	1	8	8	0.11	3.04
40	778	35.4	35.4	1	8	8	0.15	3.04
50	972	35.4	35.4	1	8	8	0.19	3.04
30	413	25	25	1	16	16	0.06	6.08
40	550	25	25	1	16	16	0.08	6.08
50	668	25	25	1	16	16	0.09	6.08

Results and Discussion

Thickness and Chemical Composition of the Coating

Both common types of contrast in SEM, SE and BSE can resolve the cemented carbide body and distinguish it from its coating. Thickness measurements using parallel lines through the entire image frame measured mean thickness values. As shown in Fig. 2, the rake face has a thicker coating than the bottom side. Coating thicknesses are 5.338 μm ± 0.240 μm and 2.978 μm ± 0.105 μm, respectively. Thicker coatings on the rake faces of these inserts endure their use phase since chips forming during machining move across these faces and cause local abrasion such as crater wear. However, surface roughness of the coatings may lead to artifacts in thickness measurements due to the introduction of topography and, by that, being highlighted in SE contrast. Such artifacts occur rather on the micrographs of the bottom side than on the rake face. From a remanufacturing perspective, it is more interesting to characterize the rake face more precisely to reach suitable decoating around crater wear.

EDX measurements help to confirm the TiN coating and identify the matrix material of the cemented carbide body. Therefore, a line spectrum and several point spectra were recorded. The line spectrum is recorded in a direction perpendicular to the insert surface and goes inward from there. As indicated by Fig. 3, the coating mainly consists of titanium and

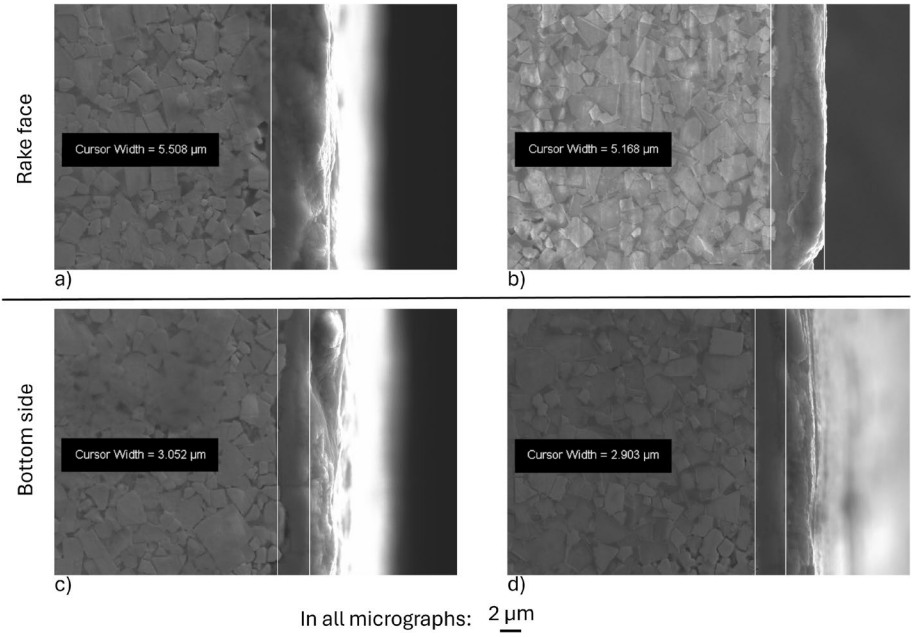

Fig. 2 SEM coating thickness measurements in SE contrast on metallographic cross-sections on TiN-coated tool inserts **a**)/**b**) rake face and **c**)/**d**) bottom side

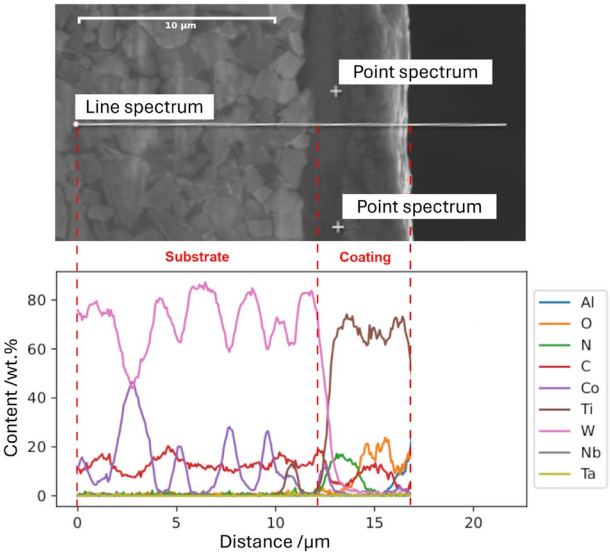

Fig. 3 Evolution of chemical composition in the tool insert as given by an EDX line spectrum

nitrogen with contaminations of oxygen and carbon next to the surface. This measurement cannot rule out the presence of titanium oxides or carbides, so some uncertainty remains.

In the transition from coating to cemented carbide body, the titanium concentration drops in favor of an increasing tungsten content, which becomes the dominant element. At a distance

of about 11 μm, the line spectrum shows a Ti-peak in the matrix. While unexpected, it can be explained by the fact that the measurement corresponds to a zone between grains, where Ti may have more easily diffused into the Co. A volatile signal as well as an inverse correlation can be observed between the W and Co contents. That is, when the amount of W in the sample decreases, the amount of Co increases (see Fig. 3 at measured distances approx. 2.5 μm, 5 μm, 7.5 μm, 10 μm). The amount of measured C also follows the same trend as W, even if less strongly and always in smaller amounts (more prominently observed at approx. 2.5 μm and 10 μm). Hence, the matrix of this cemented carbide body consists of cobalt and the inverse correlation of curve shapes results from alternations between WC particles and Co matrix along the line spectrum.

Three point spectra, two as given in Fig. 3 and one from another image, of the coating confirmed the results of the line scan. Table 4 summarizes the main elements found by EDX and gives errors. These errors were calculated using the gaussian law of error propagation on the basis of standard deviations given by EDX results. If the manufacturer declares these tool inserts had TiN coatings, it would be expected that the nitrogen content would rank second. Instead, oxygen ranks second and carbon ranks fourth with a content close to nitrogen. This points towards rather complex non-oxide ceramics than TiN. On the one hand, the increased presence of carbon in the coating could be caused by a multilayer TiN/TiC or TiN/TiCN/TiC coating. On the other hand, the manufacturer's specifications have no mention of this and TiC coatings usually have a characteristic darker copper or dark-grey colour. This would surely become visible since in this case the TiC layer would be on the outermost part of the coating. Coupled with the high amount of oxygen present, it is arguable that this carbon comes instead from contamination in one of the sample preparation steps, as well as oxidation. The polishing step in particular seems a potential candidate, as the diamond suspension and abrasive discs used could explain the increased carbon content. Escpecially the outermost part of the coating is susceptible for contamination, because mechanical polishing is known to round off edges. This particular edge formed a boundary between tool insert and resin during the metallographic preparation. Rounding off the edges may form a small crevice between tool insert and resin, where carbon from diamond particles of polishing suspensions may lead to artifacts in EDX measurements. Obviously, thorough cleaning cannot prevent these artifacts.

The obtained chemical composition of the cemented carbide body was approximately the same, consisting of a majority of W, around 10 wt.% C and some minor amounts of Co, which forms the matrix where tungsten carbide particles are embedded. Table 5 summarizes the composition of three point spectra.

Table 4 Summary of the EDX point spectra of the coating, further impurities were omitted to mention

Element	Mean content /wt.%	Error in content /wt.%
Titanium (Ti)	71.3	0.32
Nitrogen (N)	8.2	0.12
Oxygen (O)	9.7	0.29
Carbon (C)	7.5	0.09
Tungsten (W)	1.5	0.01

Table 5 Summary of the EDX point spectra of the cemented carbide body, further impurities were omitted to mention

Element	Mean content /wt.%	Error in content /wt.%
Tungsten (W)	85.5	0.32
Carbon (C)	11.6	0.19
Cobalt (Co)	1.4	0.02
Nitrogen (N)	0.0	0.23
Oxygen (O)	0.8	0.04

Laser Ablation of TiN Coatings

In order to achieve an efficient laser ablation process, the wavelength of the laser system has to meet a region of preferably high absorption within the spectrum of the ablated material. An absorption spectrum highly depends on the geometry of particles or morphology of coatings. Hence, the spectrum of TiN on a cemented tungsten carbide substrate presented by [41] is used to check on how good the laser system of this study matches the spectrum. For better understandability, the wave energy this spectrum originally had, was converted to a wavelength in Fig. 4.

As shown in Fig. 4, the wavelength used for decoating in this study is similar to literature values but slightly exceeds them. At this point of 1098 nm, a TiN-coating absorbs only 20% of the irradiated energy. It would be more efficient to harness higher absorbances as present in the UV-Vis regime. Consequently, several studies use UV-excimer lasers in that favor [36, 46]. However, this study aims to establish a low-threshold alternative for implementation and an additionally cost-efficient way to prepare coated cemented carbide tools for reconditioning and re-coating, so UV-excimer lasers are out of scope. Establishing a low-threshold alternative also means to employ industrial state of the art laser devices such as the laser engraving system of this study which is commonly used to engrave or write e.g. identifiers on technical components. Decoating results of this industrial laser engraving system may facilitate industrial adoption of this remanufacturing route by repurposing existing laser systems. Additionally, literature has already proven that less absorbance can still lead to proper ablation [11, 12, 30].

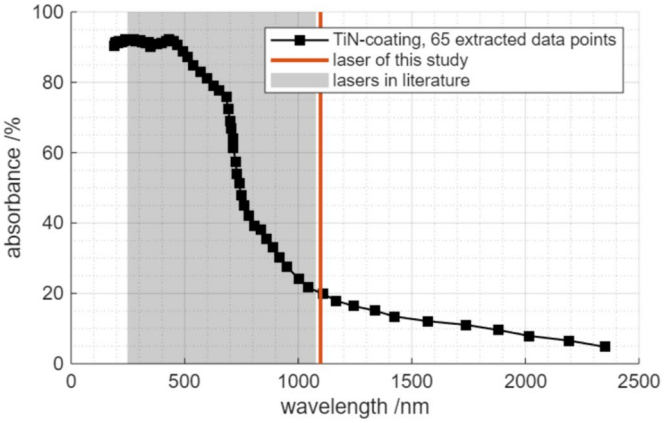

Fig. 4 Absorption spectrum of a TiN-coating on a cemented carbide substrate adapted from [41], literature wavelengths were reported in [6, 11, 12, 30, 36, 46], data extraction was performed on plotdigitizer.com

Effect of number of pulses (NOP)

The variation of number of pulses (NOP) per scan and in total displays variations of several laser parameters at once through collective parameters. Seven discrete stages of NOP were analyzed. As indicated by Fig. 5, larger NOP per scan tends to increase ablation depth. This is plausible since more laser pulses irradiate a surface increment. The mean ablation depth slightly decreases from NOP = 8 to NOP = 10, but both error bars form a large intersection and probably no effect causes this observation. Scatter also increases at higher NOP due to a strong increase in roughness. This laser engraving system provides a gaussian beam shape, so a higher NOP leads to more exposures of a surface increment to this intensity distribution. Consequently, the center of a pulsed scan track forms deeper trenches at higher NOP. Edges of scan tracks get ablated by a subsequent scan track depending on the overlap Δy, but still a higher NOP increases surface topography which result in higher roughness values as displayed in Fig. 6.

Comparably coarse surfaces providing large roughness and topography at NOP = 16 and NOP = 32 per scan raise the question, whether the coating was removed sufficiently or just locally. Therefore, EDX spectra on the ablated areas shall clarify this question. Table 6 gives

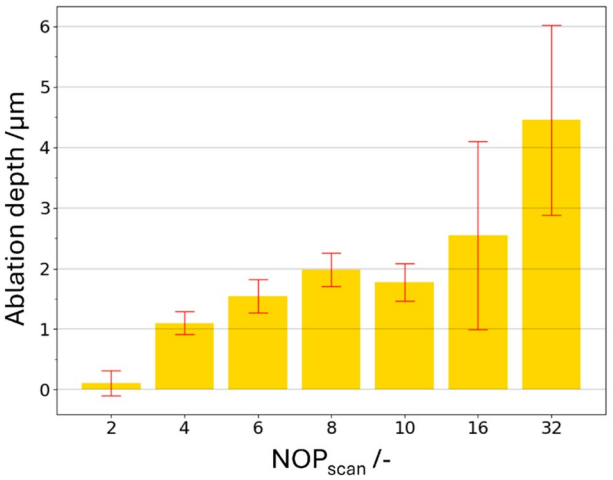

Fig. 5 Evolution of the ablation depth with increasing NOP in a single scan

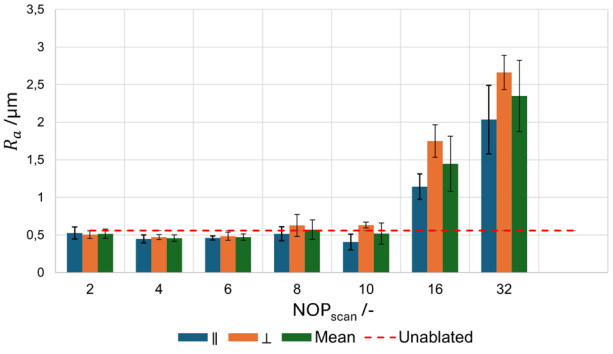

Fig. 6 Mean roughness R_a of ablated zones at different NOPs; ∥: measurement direction along scan orientation, ⊥: measurement direction perpendicular to scan orientation

Table 6 Post-ablation EDX results depending on the NOP per scan

Laser and ablation information		EDX element content		
NOP_{scan} /-	Mean depth /μm	Ti /wt.%	W /wt.%	Co /wt.%
2	0.104±0.205	97.8	0.3	1.6
4	1.099±0.190	97.6	0.6	1.4
6	1.545±0.278	97.2	1.4	1.2
8	1.985±0.274	93.8	2.9	2.4
10	1.778±0.305	80.9	13.2	5.3
16	2.547±1.549	16.6	72.4	10.8
32	4.451±1.574	5.1	78.1	13.4

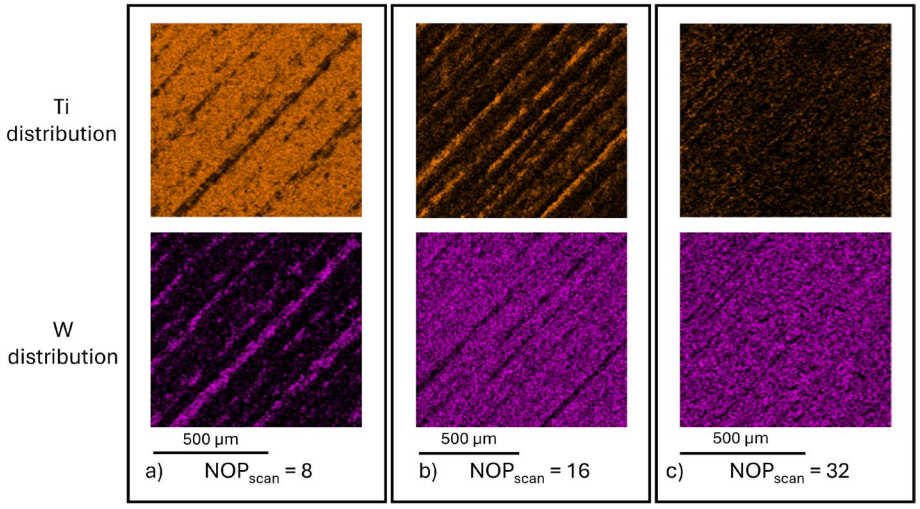

Fig. 7 Post-ablation element distributions of titanium and tungsten to assess proper decoating at a) NOP_{scan} = 8, b) NOP_{scan} = 16 and c) NOP_{scan} = 32

mean concentrations of point spectra, whereas Fig. 7 presents element maps to illustrate the underlying distributions across the irradiated areas.

From NOP_{scan} = 10 on, Ti contents decrease and the coating is gradually more removed, but still at NOP = 32 there are some residues of Ti present. Areal scans as shown in Fig. 7 support this trend by progressively decreasing titanium content (orange color) and progressively increasing tungsten content (violet color) with increasing NOP_{scan}. The element distribution maps exhibit stripe-shaped patterns referring to the pattern of laser scan tracks. At NOP_{scan} = 8, these stripes in the EDX maps, see Fig. 7 a), mark regions of comparatively deep ablation, because tungsten was detected instead of the predominant titanium. At NOP_{scan} = 16 in Fig. 7 b), stripes mark the opposite if compared to NOP_{scan} = 8 since most of the area is decoated and characterized by a high tungsten contents, but the regions of high titanium content are obviously edges of scan tracks suffering from less ablation than centers. Finally at NOP_{scan} = 32 in Fig. 7, only traces of titanium are visible in the EDX maps and maps become rather homogeneous. However, point spectra of Table 6 still detected 5.1 wt.% titanium at NOP_{scan} = 32, so increasing just the NOP per scan cannot decoat a tool insert entirely and creates at the same time large surface roughness, which might cause problems in further processing steps like reconditioning.

On the one hand, increasing the number of scans offers to harness smooth surfaces of comparatively low NOP per scan and an ablation depth which is sufficient for decoating at the same time. On the other hand, these benefits reduce the decoating rate. Figure 8 illustrates the evolution of the mean ablation depth at discrete total NOP stages at different numbers of scans. Results from the previous discussion are also included for a better comparison. In all cases the ablation depth increases upon increasing number of scans. For $\mathrm{NOP}_{total} = 16$ and $\mathrm{NOP}_{total} = 32$, scatter of the ablation depth at $n = 1$, which was discussed before to result from major roughness, exceeds scatter at every analyzed $n > 1$. Trench-shaped scan tracks are superposed by trench-shaped tracks of subsequent scans of other orientations reducing the characteristic surface topography which forms from a combination of scan pattern and beam shape. Centers of scan tracks are deeper than the edges and the rotation between scans levels surfaces. Mean roughness values of Fig. 9 c) and d) support this hypothesis. However, scatter (Fig. 8 a) and b)) and roughness (Fig. 9 a) and b)) deviates as more scans increase both. At low total NOP, the NOP per scan is small either. Consequently, the overlap of laser spots Δx inside scan tracks decreases and their spot shape has more influence than the integral track. Hence, scatter in ablation depth and values of R_a increase upon the formation of topography inside scan tracks. Multiple scans obviously tend to promote this topography formation instead of smoothing as it occurred at higher NOPs.

Again, EDX point spectra and element distribution maps clarify whether the coating was removed completely. With $\mathrm{NOP}_{total} = 16$ detected titanium contents begin to drop in Table 7. However, $\mathrm{NOP}_{total} = 32$ at $n = 8$ is the only tested parameter that removes the

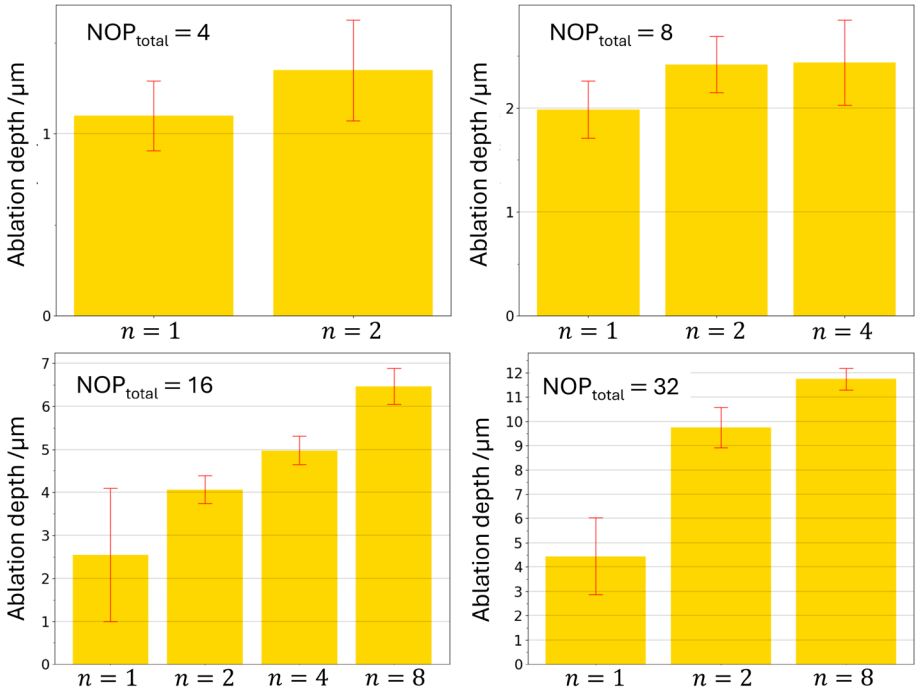

Fig. 8 Mean ablation depth of different numbers of scans at **a)** $\mathrm{NOP}_{total} = 4$, **b)** $\mathrm{NOP}_{total} = 8$, **c)** $\mathrm{NOP}_{total} = 16$ and d) $\mathrm{NOP}_{total} = 32$

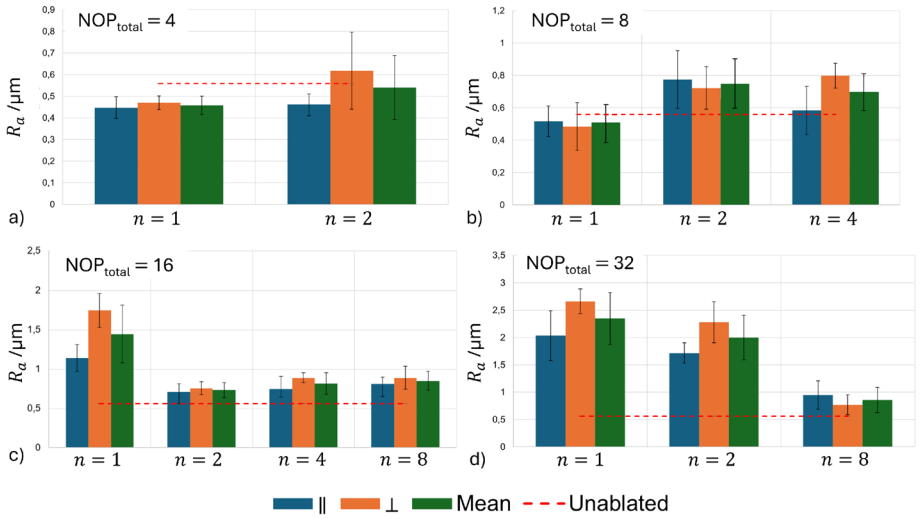

Fig. 9 Mean roughness R_a of ablated zones for different numbers of scans at **a)** NOP$_{total} = 4$, **b)** NOP$_{total} = 8$, **c)** NOP$_{total} = 16$ and d) NOP$_{total} = 32$; ∥: measurement direction along scan orientation, ⊥: measurement direction perpendicular to scan orientation

Table 7 Post-ablation EDX results at different NOPs and number of scans

Laser and ablation information			EDX element content		
NOP$_{total}$ /-	Mean depth /μm	n /-	Ti /wt.%	W /wt.%	Co /wt.%
4	1.099±0.190	1	97.6	0.6	1.4
4	1.351±0.277	2	97.4	0.7	1.3
8	1.985±0.274	1	93.8	2.9	2.4
8	2.419±0.270	2	93.2	2.1	2.7
8	2.437±0.412	4	92.9	3.6	2.4
16	2.547±1.549	1	16.6	72.4	10.8
16	4.066±0.318	2	37.2	53.0	9.3
16	4.976±0.334	4	12.0	77.3	10.0
16	6.466±0.442	8	8.3	81.7	9.5
32	4.451±1.574	1	5.1	78.1	13.4
32	9.752±0.826	2	1.2	82.7	15.1
32	11.740±0.449	8	0	90.4	9.6

coating entirely from a tool insert. Element distribution maps in Fig. 10 clearly show that the titanium content decreases progressively and is finally entirely removed. Based on the presented results, decoating of tools with this laser engraving system works best with an total NOP of 32 at 8 scans. With respect to the corresponding mean ablation depth, this parameter set removes more than just the coating, while only 2 scans at the same NOP$_{total}$ decoat to a depth where the transition between coating and cemented carbide body is. However, 8 scans are favorable to reduce surface roughness in order to save time and resources in a subsequent reconditioning process of the decoated regions.

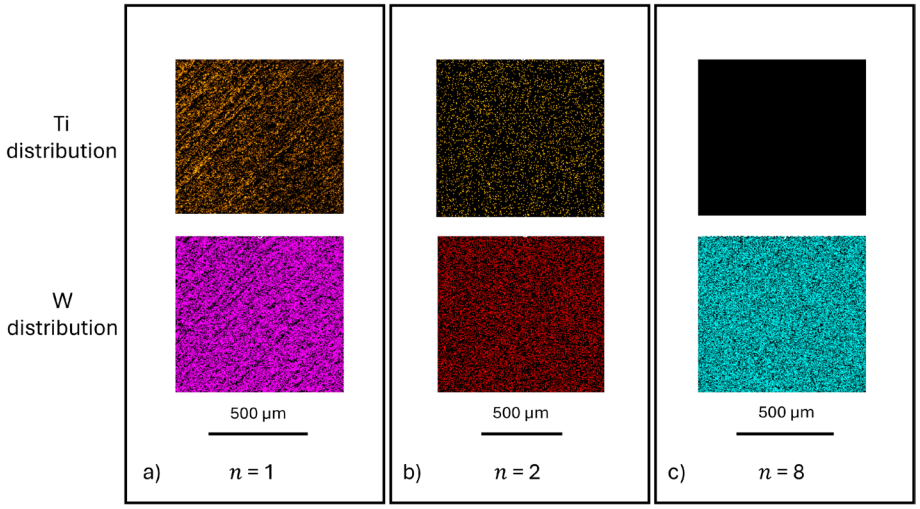

Fig. 10 Post-ablation element distributions of titanium and tungsten to assess proper decoating at $\mathrm{NOP}_{total} = 32$ and different numbers of scans **a**) $n = 1$, **b**) $n = 2$ and **c**) $n = 8$

Effect of Pulse Frequency

Two discrete NOP values, 8 and 16 at $n = 1$, were chosen to be kept constant upon the variation of the pulse frequency during laser decoating. Its effect on the mean ablation depth is summarized in Fig. 11. For NOP = 8, there is an almost negligible change in the mean depth and error bars overlap whereas for NOP=16 a higher frequency amounts to a reduced ablation depth. This reduced depth is thought to be a direct consequence of the reduced energy density brought by increasing the frequency and thus reducing the energy per pulse. However, this seems contradictory with the fact that for NOP = 8 the change in depth is almost negligible, but the effect of energy reduction per pulse gains influence with increasing NOP, which denotes the number of pulses per surface increment. Consequently, the total energy input decreases stronger at NOP = 16 than at NOP = 8.

Regarding the mean roughness R_a of the ablated zone, Fig. 12 shows an example for each pulse frequency and NOP = 8 or NOP = 16, respectively. Roughness parameters were

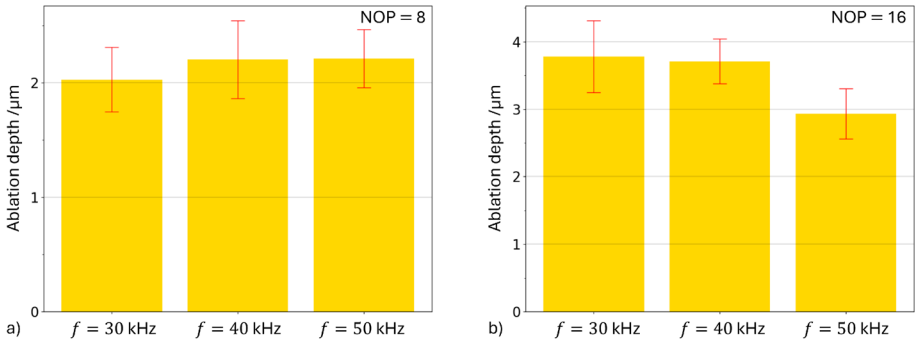

Fig. 11 Effect laser pulse frequency during decoating of a TiN tool insert at a) NOP = 8 and b) NOP = 16

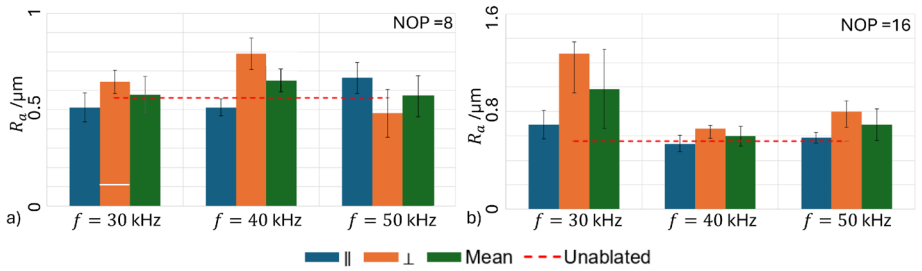

Fig. 12 Mean roughness R_a of ablated zones at a) NOP = 8 and b) NOP = 16; ||: measurement direction along scan orientation, ⊥: measurement direction perpendicular to scan orientation

Table 8 Post-ablation EDX point spectra to confirm sufficient decoating

Laser and ablation information			EDX element content		
NOP /-	Depth /μm	f /kHz	Ti /wt.%	W /wt.%	Co /wt.%
8	2.026±0.281	30	89.3	3.9	5
8	2.203±0.340	40	95.9	1.8	2.0
8	2.211±0.254	50	96.2	0.8	1.7
16	3.780±0.535	30	22.4	64.5	11.9
16	3.709±0.330	40	63.9	27.3	7.0
16	2.931±0.974	50	85	9.2	3.8

extracted from 3D images using the digital microscope. Regarding the measured R_a values, a pulse frequency of 30 kHz leads to the worst surfaces which are rougher than before ablation. Frequencies of 40 kHz and 50 kHz are similar to the roughness of the pristine coating or do even undercut it. However, the roughness after 30 kHz decoating has a manageable increase if compared to the unablated state.

In order to assess, whether the coating was entirely removed, EDX scans of the ablated areas were performed. If so, tungsten or cobalt contents should exceed titanium contents by far. Table 8 contains only one ablation where this seems to be the case and this has the deepest ablation. All the other ablations require more scans to result in decoated tools. So, 30 kHz is chosen as the pulse frequency to remove TiN coatings.

Optimal Laser Decoating Parameter Set

A combination of ablation depth, success in decoating and surface roughness after laser irradiation identifies suitable laser parameters. The only proof of success in decoating is given at $\mathrm{NOP}_{total} = 32$ with 8 scans at 30 kHz pulse frequency. Variations in pulse frequency support 30 kHz as the most sufficient for decoating. Even if for this total NOP the influence of pulse frequency was not investigated, the NOP per scan exceeded the NOP per scan of the aforementioned optimum and other pulse frequencies still could not remove the coating. Therefore, the optimum laser decoating parameter set for the 30 W IR laser engraving system uses the settings given in Table 9.

Table 9 Optimal laser decoating parameter set for this laser engraving system; extracted from Table 3

f /kHz	v /mm/s	Δx /%	Δy /%	n /-	NOP/scan	NOP_{total}	r_{decoat} /cm^2/s
30	825	50	50	8	4	32	0.03

Emission Savings

The following considerations are rather rough estimations than exact calculations. Amounts of primarily electrical energy are estimated for the production of a new tool insert and the beginning of a remanufacturing chain of worn ones. There is a comparison between sintering of a preexisting green body of WC-Co and laser decoating of an entire tool insert face, omitting raw material production, transport, the entire coating procedure and scaling effects of mass production. As reported by the [13], producing 1 kWh of electricity emits an average of 210 g CO_2e (grams of carbon dioxide equivalents) in the European Union. This value allows to transform the obtained energy into emission under the assumption that all energy used is electricity.

[8] report a time temperature profile of sintering cemented carbides as illustrated in Fig. 13. Only the heating program is taken into account. In an approximation for simpler calculations, this time temperature profile, which consists of several heating and dwelling sections, is considered as an only heating profile at constant rate as indicated by the dashed line. If the energy consumed during sintering depends on the integral of the temperature over time, this approximation underestimates the real energy consumption. Additionally, energy requirements to establish sintering atmospheres are neglected, either.

The energy consumption to produce a new tool insert E_{new} is considered to arise from a change in enthalpy to trigger sintering corrected by a degree of efficiency of an industrial oven. It depends on:

- Mass of a tool insert $m = 6.03$ g, the mean mass of the tool inserts in this study, weighed on a precision balance AT200 (Mettler Toledo, Columbus, Ohio, USA)
- Specific heat capacity $c_p = 0.35 \ \frac{\mathrm{J}}{\mathrm{g\,K}}$ as an average from [47] while omitting its temperature dependency
- Total temperature difference $\Delta T = T_{sinter} - T_{room} = 1723 \ \mathrm{K} - 293 \ \mathrm{K} = 1430 \ \mathrm{K}$ according to [8]

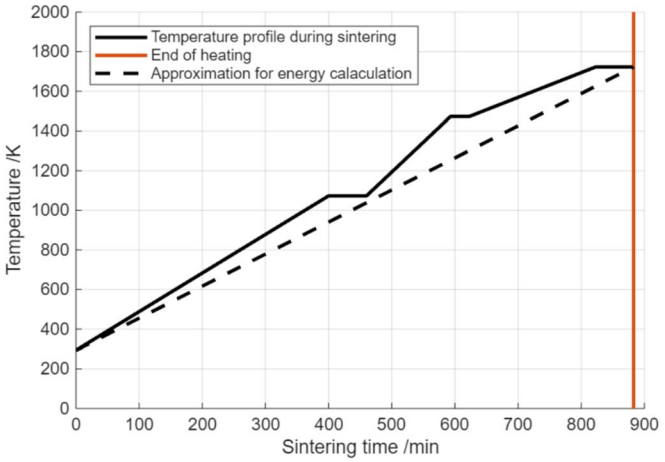

Fig. 13 Exemplary sintering program for WC-Co cemented carbides according to [8] including a linear all-heating approximation

Table 10 Estimations of energy consumption and emissions caused by new production and remanufacturing of tool inserts and possible savings

	New insert	remanufactured insert
Energy consumption per insert /Wh	5.59	1.67
Emission per insert /g CO_2e	1.17	0.35
Savings remanufactured compared to new	−70.2%	

- Degree of efficiency $\eta_{oven} = 0.15$ of an oven, a rough estimation depending on the oven type and its utilization according to [53]

Joined together in one equation, it is:

$$E_{new} = \frac{1}{\eta_{oven}} \, m \, c_p \, \Delta T \tag{1}$$

The energy consumption of laser decoating E_{decoat} depends on the laser power $P = 30$ W, the duration of the decoating process $t_{decoat} = 120$ s for the entire insert and the degree of efficiency of the laser system $\eta_{laser} \approx 0.6$ [4]. It is:

$$E_{decoat} = \frac{1}{\eta_{laser}} \, P \, t_{decoat} \tag{2}$$

Energy consumption and CO_2-emission of both, new production and remanufacturing without reconditioning and re-coating are presented in Table 10. CO_2-emissions result from multiplication of energy consumption and emission per kWh of electricity in the European Union.

As stated in Table 10, remanufacturing can save 70.2% of energy if compared to new production of tool inserts even though numerous contributors to energy consumption and emission were neglected. This rough estimation proved large potential not only to save energy, but save emissions and money either. Hence, remanufacturing of tool inserts with decoating as a first step can increase the overall efficiency and sustainability of tool inserts. It is expected, that larger tools are even more worthwhile for remanufacturing, because they probably require longer and, by that, more energy during their sintering processes to achieve joining in their core.

Conclusion and Future Research

This study investigated the removal of hard ceramic coatings from cemented carbide milling inserts. If compared to literature, lower laser power was used to achieve optimal decoating results of TiN coated cemented carbide inserts. A commercial laser engraving system was used as a low cost alternative to expensive excimer lasers which are frequently used in laboratory experiments (see Table 1). The key findings are:

- Decoating at lower laser power than reported in literature is possible. In this study, 30 W sufficed to remove a 5 μm TiN coating.
- The optimal laser decoating parameter set operates at 30 kHz pulse frequency, 30 W

laser power, 825 mm/s scan speed as well as 50% offset between laser spots inside one track (Δx) and between tracks (Δy). The number of scans is 8 and the rotation between subsequent scans is 22.5°.

- These parameters lead to a decoating rate of 0.03 cm^2/s. In contrast to the more scientific ablation rate expressing an ablation depth per pulse, this one includes the lead time to decoat a predefined surface area. So, the size of regions which are necessary to be decoated for reconditioning processes is linked directly to the duration of ablation. It takes about 2 minutes to decoat such an insert entirely.
- If compared to the production of a new cemented carbide body, laser decoating of an entire insert saves 70.2% of required energy. This also applies to emission savings under the assumption that the entire energy consumed is electricity. Savings mainly arise from avoiding multi-stage sintering processes required during production of new inserts. However, energy savings can further increase if predefined regions around wear are decoated selectively instead of decoating entire inserts.

Future studies should investigate various types of wear and the challenges their topography poses to laser decoating. Depending on subsequent reconditioning processes of cutting edges like grinding or another laser ablation as proposed by [21], relevant regions around wear have to be defined to harness the selectivity of laser decoating. The minimum surface area to decoat will then lead to the fastest decoating process. These are probably key factors to develop an economically viable remanufacturing process chain.

Supplementary Information

Supplementary information is made available upon request to the authors.

Acknowledgements This research was generously funded by the European Regional Development Fund (ERDF) and the state government of Saarland in the project PSS4CE - product service systems for a circular economy. The authors thank the chair of Prof. Dr. Christian Motz (Department of Materials Science and Technology) for the help with all SEM and EDX measurements as well as Marco Busse at TecMan Saar GmbH for the assistance with laser ablation experiments.

Funding Open Access funding enabled and organized by Projekt DEAL.

Declarations

Competing interests All authors declare to have no competing interests.

References

1. Abele E, Ellermeier A, Hohenstein J et al (2007) Tool length influence on wear behaviour of twisted carbide drills. Prod Eng Res Devel 1(1):51–56. https://doi.org/10.1007/s11740-007-0029-5
2. Alvarez-Risco A, Rosen MA, Del-Aguila-Arcentales S (2022) Towards a Circular Economy: Transdisciplinary Approach for Business. CSR Sustainability Ethics & Governance Springer International Publishing Cham. https://doi.org/10.1007/978-3-030-94293-9
3. Assurin SR, Mativenga P, Rajab F et al (2021) Laser de-coating of hard DLC coatings from tungsten carbide cutting tool. Proceed Institut Mechan Eng Part B J Eng Manuf 235(1):13–22. https://doi.org/10.1177/0954405420962389
4. Barnes NP (2007) Solid-State Lasers From an Efficiency Perspective. IEEE J Sel Top Quantum Electron 13(3):435–447. https://doi.org/10.1109/JSTQE.2007.895280
5. Bonacchi D, Rizzi G, Bardi U et al (2003) Chemical stripping of ceramic films of titanium aluminum nitride from hard metal substrates. Surf Coat Technol 165(1):35–39. https://doi.org/10.1016/S0257-8972(02)00720-X
6. Bonse J, Sturm H, Schmidt D et al (2000) Chemical, morphological and accumulation phenomena in ultrashort-pulse laser ablation of TiN in air: Appl Phys A Mater Sci Process 71(6):657–665. https://doi.org/10.1007/s003390000585
7. Cermak A, Kozmin P, Research & Development, HOFMEISTER sro, Pilsen, Czech Republic, et al. (2022) Segmental laser stripping of thin coatings on monolithic cutting tools. MM Sci J 2022(4):6007–6013. https://doi.org/10.17973/MMSJ.2022_11_2022126
8. Chen CS, Yang CC, Chai HY et al (2014) Novel cermet material of WC/multi-element alloy. Int J Refract Metal Hard Mater 43:200–204. https://doi.org/10.1016/j.ijrmhm.2013.11.005
9. Company KJL (2018) Safety Data Sheet Titanium Oxides
10. Davim JP (2008) Machining. Springer London London. https://doi.org/10.1007/978-1-84800-213-5
11. Demir AG, Pangovski K, O'Neill W et al (2015) Investigation of pulse shape characteristics on the laser ablation dynamics of TiN coatings in the ns regime. J Phys D Appl Phys 48(23):235202. https://doi.org/10.1088/0022-3727/48/23/235202
12. Deng J, Li S, Xing Y et al (2014) Studies on thermal shock resistance of TiN and TiAlN coatings under pulsed laser irradiation. Surf Eng 30(3):195–203. https://doi.org/10.1179/1743294413Y.0000000236
13. European Environment Agency (EEA) (2024) Greenhouse gas emission intensity of electricity generation in Europe
14. Ferraris E, Mestrom T, Bian R et al (2012) Machinability Investigation on High Speed Hard Turning of ZrO2 with PCD Tools. Procedia CIRP 1:500–505. https://doi.org/10.1016/j.procir.2012.04.089
15. Flehmke M, Hinrichs M, Möller C et al (2024) Cutting Carbon Footprint With Smart Tool Management And Cemented Carbide (WC-Co) Upcycling. https://doi.org/10.15488/17764
16. Fonseca AS, Viana M, Querol X et al (2015) Workplace Exposure to Process-Generated Ultrafine and Nanoparticles in Ceramic Processes Using Laser Technology. In: Viana M (ed) Indoor and Outdoor Nanoparticles, vol 48. Springer International Publishing, Cham, pp 159–179. https://doi.org/10.1007/698_2015_422
17. Furberg A, Fransson K, Zackrisson M et al (2020) Environmental and resource aspects of substituting cemented carbide with polycrystalline diamond: The case of machining tools. J Clean Prod 277:123577. https://doi.org/10.1016/j.jclepro.2020.123577
18. García J, Collado Ciprés V, Blomqvist A et al (2019) Cemented carbide microstructures: A review. Int J Refract Metal Hard Mater 80:40–68. https://doi.org/10.1016/j.ijrmhm.2018.12.004
19. Glaser A, Surnev S, Netzer F et al (2007) Oxidation of vanadium nitride and titanium nitride coatings. Surf Sci 601(4):1153–1159. https://doi.org/10.1016/j.susc.2006.12.010
20. Hazzan KE, Pacella M (2022) A novel laser machining strategy for cutting tool repair. Manufactur Lett 32:87–91. https://doi.org/10.1016/j.mfglet.2022.04.005
21. Hazzan KE, Pacella M (2022) Surface defect detection and prediction in carbide cutting tools treated by lasers. Procedia CIRP 108:851–856. https://doi.org/10.1016/j.procir.2022.05.198
22. Hazzan KE, Pacella M, See TL (2021) Laser Processing of Hard and Ultra-Hard Materials for Micro-Machining and Surface Engineering Applications. Micromachines 12(8):895. https://doi.org/10.3390/mi12080895
23. Inc. MAC (2023) Safety Data Sheet Titanium Nitride Powder
24. Intanon N, Wisitsoraat A, Saikaew C (2022) An application of statistical quality tools for process robustness and sustainability of titanium nitride coating on a machine component of a fishing net weaving machine. J Clean Prod 363:132603. https://doi.org/10.1016/j.jclepro.2022.132603
25. IonBondLLC (2014) Safety Data Sheet Titanium Carbonitride

26. Ivanov V, Evtuhov A, Dehtiarov I et al (2025) Fundamentals of Manufacturing Engineering Using Digital Visualization. Springer Tracts in Mechanical Engineering Springer Nature Switzerland Cham. https://doi.org/10.1007/978-3-031-74360-3
27. Kang K, Su S, Yu B et al (2025) The review and prospect of tool coating technology. Intern J Adv Manuf Technol 137(7–8):3107–3139. https://doi.org/10.1007/s00170-025-15344-x
28. Ke M, Shao L, Chen Y et al (2025) Surface pretreatment methods for cemented carbide substrates of the coated cutting tools: A review. Precis Eng 96:663–691. https://doi.org/10.1016/j.precisioneng.2025.07.019
29. Klocke F (2011) Manufacturing Processes 1: Cutting. RWTHedition Springer Berlin Heidelberg Berlin Heidelberg. https://doi.org/10.1007/978-3-642-11979-8
30. Kononenko T, Garnov S, Pimenov S et al (2000) Laser ablation and micropatterning of thin TiN coatings. Appl Phys A Mater Sci Process 71(6):627–631. https://doi.org/10.1007/s003390000572
31. Krishna PV, Mohanty UK (2025) Effect of Machining Parameters on Machining Performance during End Milling. Sadhānā 50(1):13. https://doi.org/10.1007/s12046-024-02639-0
32. Kücher G, Luidold S, Czettl C et al (2018) Lixiviation kinetics of cobalt from cemented carbides. Int J Refract Metal Hard Mater 70:239–245. https://doi.org/10.1016/j.ijrmhm.2017.10.004
33. Kundrák J, Fedorovich V, Pyzhov I et al (2019) Improving the effectiveness of combined grinding processes for processing superhard materials. J Manuf Process 43:270–275. https://doi.org/10.1016/j.jmapro.2019.05.004
34. Liang J, Gao H, Xiang S et al (2022) Research on tool wear morphology and mechanism during turning nickel-based alloy GH4169 with PVD-TiAlN coated carbide tool. Wear 508–509:204468. https://doi.org/10.1016/j.wear.2022.204468
35. LLC AM (2018) Safety Data Sheet Titanium Carbide
36. Marimuthu S, Kamara AM, Whitehead D et al (2011) Laser stripping of TiAlN coating to facilitate reuse of cutting tools. Proceed Institut Mechan Eng Part B-J Eng Manuf 225(B10):1851–1862. https://doi.org/10.1177/0954405411414313
37. Patel GCM, Chate GR, Parappagoudar MB et al (2020) Machining of Hard Materials: A Comprehensive Approach to Experimentation. SpringerBriefs in Applied Sciences and Technology, Springer International Publishing, Cham, Modeling and Optimization. https://doi.org/10.1007/978-3-030-40102-3
38. Pliatsikas N, Panos S, Odutola T et al (2024) Colloidal Titanium Nitride Nanoparticles by Laser Ablation in Solvents for Plasmonic Applications. Nanomaterials 14(14):1214. https://doi.org/10.3390/nano14141214
39. Primus T, Hlavinka J, Zeman P et al (2021) Investigation of Multiparameter Laser Stripping of AlTiN and DLC C Coatings. Materials 14:951. https://doi.org/10.3390/ma14040951
40. Primus T, Hlavinka J, Zeman P et al (2023) Experimental Investigation of a Method for Selective and Precise Laser De-Coating. Lasers Manuf Mater Process. https://doi.org/10.1007/s40516-023-00202-z
41. Rahman MM, Jiang ZT, Munroe P et al (2016) Chemical bonding states and solar selective characteristics of unbalanced magnetron sputtered $Ti_x M_{1-x-y} N_y$ films. RSC Adv 6(43):36373–36383. https://doi.org/10.1039/C6RA02550A
42. Sousa VFC, Da Silva FJG, Pinto GF et al (2021) Characteristics and Wear Mechanisms of TiAlN-Based Coatings for Machining Applications: A Comprehensive Review. Metals 11(2):260. https://doi.org/10.3390/met11020260
43. Straffelini G (2015) Friction and Wear: Methodologies for Design and Control. Springer Tracts in Mechanical Engineering Springer International Publishing Cham. https://doi.org/10.1007/978-3-319-05894-8
44. Sun Y, Sun J, Li J et al (2013) Modeling of cutting force under the tool flank wear effect in end milling Ti6Al4V with solid carbide tool. Intern J Adv Manuf Technol 69(9–12):2545–2553. https://doi.org/10.1007/s00170-013-5228-y
45. Sun Y, Sun J, Wang G et al (2020) A modified analytical cutting force prediction model under the tool crater wear effect in end milling Ti6Al4V with solid carbide tool. Intern J Adv Manuf Technol 108(11–12):3475–3490. https://doi.org/10.1007/s00170-020-05579-1
46. Sundar M, Mativenga PT, Li L et al (2009) Laser removal of TiN from coated carbide substrate. Intern J Adv Manuf Technol 45(11):1169. https://doi.org/10.1007/s00170-009-2059-y
47. Tan J, Wen S, Liu Y et al (2023) Thermal conductivity of WC-Co-TiC cemented carbides: Measurement and modeling. Int J Refract Metal Hard Mater 112:106153. https://doi.org/10.1016/j.ijrmhm.2023.106153
48. ThermoFisherUK (2024) Safety Data Sheet Titanium Nitride
49. Toboła D, Czechowski K, Wrońska I et al (2013) The effects of the coating stripping process on regenerated tool cutting edges. J Achiev Mater Manuf Eng 61:294–301
50. Toros A, Kiss M, Graziosi T et al (2020) Reactive ion etching of single crystal diamond by inductively coupled plasma: State of the art and catalog of recipes. Diam Relat Mater 108:107839. https://doi.org/10.1016/j.diamond.2020.107839

51. Vlasova M, Alimbekov M, Zhelezov P et al (2020) Laser-induced Si3N4-TiN ceramics degradation. Ceram Int 46(3):3668–3674. https://doi.org/10.1016/j.ceramint.2019.10.087
52. Wongsisa S, Srichandr P, Poolthong N (2015) Development of Manufacturing Technology for Direct Recycling Cemented Carbide (WC-Co) Tool Scraps. Mater Trans 56(1):70–77. https://doi.org/10.2320/matertrans.M2014213
53. Zhao J, Ma L, Zayed ME et al (2021) Industrial reheating furnaces: A review of energy efficiency assessments, waste heat recovery potentials, heating process characteristics and perspectives for steel industry. Process Saf Environ Prot 147:1209–1228. https://doi.org/10.1016/j.psep.2021.01.045